Linker Effects on Monolayer Formation and Long-Range Electron Transfer in Helical Peptide Monolayers

Yoko Arikuma, Kazuki Takeda, Tomoyuki Morita, Masashi Ohmae, and Shunsaku Kimura*

Department of Material Chemistry, Graduate School of Engineering, Kyoto University, Kyoto-Daigaku-Katsura, Nishikyo-ku, Kyoto 615-8510, Japan

Received: November 20, 2008; Revised Manuscript Received: February 15, 2009

Helical peptides carrying a ferrocene unit at the C-terminus were immobilized on gold at the N-terminus via three different linkers to form self-assembled monolayers, and the long-range electron transfer from the ferrocene unit to gold was electrochemically studied. The linkers are 4-thiobenzoic acid, 3-fluoro-4-thiobenzoic acid, and 2-methoxy-4-thiobenzoic acid. All the peptides formed a monolayer with vertical orientation but some differences in monolayer packing and ferrocene surface density as they formed. However, the treatment with dodecanethiol in a gas phase uniformed to show similar monolayer physical parameters, and the electron-transfer rate constants were reproducibly obtained as well. These three peptide monolayers exhibited the same electron-transfer rate constants despite three linkers with different oxidation potentials. On the other hand, the electron transfer was decelerated seemingly by reducing the ferrocene surface density. Theoretical calculations with simple models demonstrated that the experimental result supports a hopping mechanism rather than electron tunneling though it cannot be fully excluded.

Introduction

Electron transfer through peptide secondary structures has been of great interest with regard to efficient electron transport in biological systems.[1−6] Especially, electron transfer through helical structures has attracted much attention because helices are considered to play an essential role in mediating electrons and controlling electron transfer directions in protein assemblies.[7] There have been a great number of studies on electron transfer through a model helical peptide by radiolysis[8,9] and quenching experiments[10] in solution, electrochemistry on peptide monolayers on metal surfaces,[11−17] and recently scanning probe microscopy on a single or small number of peptide molecules on a metal surface.[18−20] Several interesting features have been revealed. First, a helical peptide is a good electron mediator for electron tunneling. Its decay constant over the electron-tunneling distance is smaller ($\beta = 0.5-0.7$ Å^{-1})[10,18,20−22] than that of a hydrocarbon chain ($\beta = 0.8-1.1$ Å^{-1}).[23−26] The better electron mediation property is explained by successive semi-conjugated amide groups via hydrogen bonds along a helical peptide chain. Second, the dipole of a helical peptide affects the electron transfer. Unidirectional arrangement of the amide groups of a 3.5 D dipole forms a macrodipole as a whole with a partial positive charge at the N-terminus and negative charge at the C-terminus. The dipole effect on the electron transfer, which is acceleration in the direction from the C-terminus to the N-terminus, and deceleration in the opposite direction through the electric field generated by the dipole, has been demonstrated in solution[27,28] and in self-assembled monolayers.[15,19,29−31] Third, when the electron-transfer distance exceeds a certain point, the electron-transfer mechanism switches from simple electron tunneling to other mechanisms characterized with weak distance dependence. Extremely small decay constants at a long distance have been reported: 0.18 Å^{-1} for helical oligoprolines,[32] 0.02−0.04 Å^{-1} for α-helical peptides,[17] and 0.05 Å^{-1} for collagen-like triple helices.[33] Two mechanisms have been proposed to account for these experimental observations. One is a hopping mechanism in which a charge is injected from the donor into the intervening sites (possibly amide groups) and hops among them to reach the acceptor.[11,12,17,32,34−37] While the electron tunneling shows exponential distance dependence,[38] in the hopping mechanism the electron transfer rate constant is inversely proportional to the electron-transfer distance.[34,35,38−46] The other is a molecular motion-assisted electron transfer mechanism in which a peptide bridge thermally fluctuates to accelerate the electron transfer.[6,14,16,33,47] The combination of the two, a molecular-motion assisted hopping mechanism, is also discussed to plausibly occur.[48]

Self-assembled monolayers (SAMs) of redox-terminated helical peptides on a gold surface via a Au−S linkage have been intensively studied on the electron transfer through a helical peptide.[6,11,12,14,15,17,33,47−49] In such SAMs, the chemical structure of the linker that connects the helical peptide to the gold surface influences the overall electron transfer between the redox unit and gold. In our previous study, changing the linker at the peptide N-terminus from lipoic acid composed of a disulfide group and methylene groups to thiobenzoic acid remarkably accelerated the electron transfer reaction.[12] The enhancement of the reaction can be explained from physical and electronic aspects. First, the linker structure influences the monolayer qualities such as molecular orientation, monolayer packing, molecular dynamics, and peptide surface density to change the electron transfer rate.[14,16,33,48] Second, the electronic structure of the linker modifies the electronic coupling between the redox unit and gold to affect the probability of electron tunneling when electron tunneling is the case. These several factors should be taken into consideration for understanding the electron transfer reaction in the SAMs. Without paying attention to these points, we cannot illustrate the whole mechanism of the electron transfer reaction at the interface, which is an indispensable knowledge for development of molecular devices such as a molecular

* To whom correspondence should be addressed. Tel: +81-75-383-2400. Fax: +81-75-383-2401. E-mail: shun@scl.kyoto-u.ac.jp.

10.1021/jp810200x CCC: $40.75
Published on Web 04/10/2009

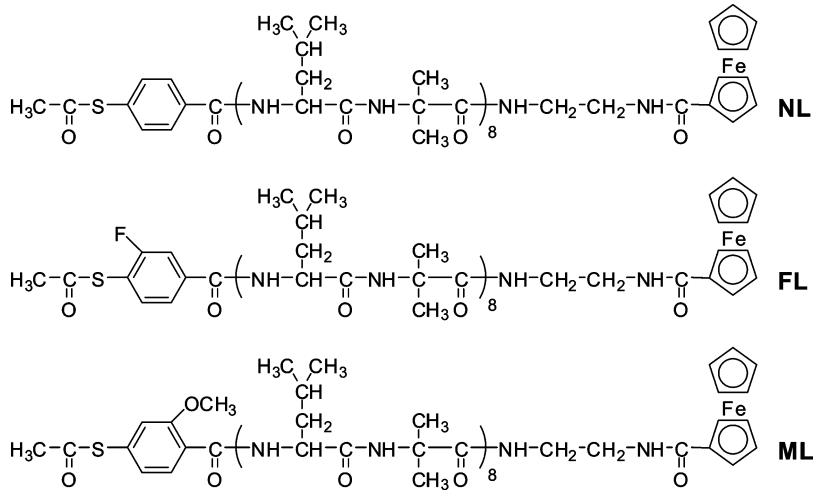

Figure 1. Chemical structures of the helical peptides.

rectifying diode,[50,51] photodiode,[29−31,52,53] and switch[54−56] on a gold surface.

In this study, we synthesized helical peptides carrying a redox-active ferrocene unit at the C-terminus and three different linkers at the N-terminus for immobilization to gold (NL, FL, and ML in the acetyl-protected form; Figure 1). The peptides were immobilized on a gold surface to prepare helical peptide SAMs, and the linker effects on the long-range electron transfer between the ferrocene unit and gold were studied. The linkers are nonsubstituted 4-thiobenzoic acid (NL), 3-fluoro-4-thiobenzoic acid (FL), and 2-methoxy-4-thiobenzoic acid (ML), which were designed to have different molecular orbital energies. Ferrocene is the most widely used to study electron transfer reactions through SAMs.[25,57−61] The peptide chain is a 16mer of an alternating sequence of L-leucine (Leu) and α-aminoisobutyric acid (Aib). This sequence is known to form a stable α-helix and self-assemble into a well-packed monolayer through interdigitation among the side chains.[11,62,63] The monolayers were characterized by infrared reflection−absorption spectroscopy (IRRAS), ellipsometry, and electrochemical blocking experiments, and the electron transfer between the ferrocene unit and gold was studied by cyclic voltammetry (CV), chronoamperometry (CA), and electrochemical impedance spectroscopy (EIS). To uniform the physical properties of the three different SAMs as similar as possible, the monolayer defects were filled in with dodecanethiol, a process that is also effective to obtain reproducible data on the electron transfer reaction. The electron transfer rate constants are obtained and discussed with theoretical calculations in terms of electron tunneling and hopping mechanisms. Furthermore, the dependences of the electron transfer on the molecular orientation, monolayer packing, and ferrocene surface density are also discussed.

Materials and Methods

Synthesis of Helical Peptides. The helical peptides, NL, FL, and ML, were synthesized by the conventional liquid-phase method. The Leu-Aib 16mer with a ferrocene unit at the C-terminus was synthesized according to the literature.[11,12,17,63] Respective acetyl-protected linkers were synthesized and coupled to the N-terminus of the peptide to obtain the final products. All the intermediates were identified by ^{1}H NMR spectroscopy, and the final products were further confirmed by FAB mass spectrometry. The purity of the compounds was checked by thin-layer chromatography (TLC). The synthetic details of the linkers and the identification data of the final products are shown below.

4-Acetylthiobenzoic Acid. To a dispersion of 4-thiobenzoic acid (100 mg) in diethyl ether/dichloromethane (1/1 v/v, 10 mL) were added *N*,*N*-diisopropylethylamine (DIEA, 170 μL) and acetic anhydride (89 μL) at 0 °C. The solution was stirred under N_2 atmosphere for 9 h with a gradual increase the temperature up to room temperature. The solution was diluted with diethyl ether and washed with 0.5 N aq HCl, and the organic layer was dried over anhydrous $MgSO_4$. The $MgSO_4$ was filtered off, and the filtrate was evaporated to afford the product (118 mg, 92.5%). ^{1}H NMR ($CDCl_3$, 400 MHz): δ(ppm) 2.38 (3H, s, CH_3CO), 7.29, 7.93 (4H, d, C_6H_4).

3-Fluoro-4-acetylthiobenzoic Acid. To a solution of 3,4-difluorobenzaldehyde (1.00 g) in chlorobenzene (10 mL) was added tetra-*n*-butylammonium bromide (46 mg), and the solution was stirred at room temperature for a while. Potassium thioacetate (884 mg) dispersed in water (3 mL) was added dropwise to the solution for 10 min. After being stirred for 1 h at room temperature, the solution was heated up to 80 °C and stirred for 8 h. The solution was diluted with chloroform and washed with water and brine, and the organic layer was dried over anhydrous $MgSO_4$. The $MgSO_4$ was filtered off, and the filtrate was evaporated. The obtained residue was purified by silica gel column chromatography (eluants: *n*-hexane and then *n*-hexane/ethyl acetate = 20/1 v/v) to afford 3-fluoro-4-acetylthiobenzaldehyde (208 mg, 15%). The product (100 mg) was dissolved in *tert*-butyl alcohol/water (4/1 v/v, 25 mL), and 2-methyl-2-butene (282 μL), NaH_2PO_4 (96 mg), and $NaClO_2$ (194 mg) were successively and slowly added to the solution. The solution was stirred at room temperature for 3 h. After reaction, the pH of the solution was adjusted to 2.0 with 4 wt% aq $KHSO_4$. The solution was diluted with chloroform and washed with brine, and the organic layer was dried over anhydrous $MgSO_4$. The $MgSO_4$ was filtered off, and the filtrate was evaporated. The obtained residue was purified by silica gel column chromatography (eluants: chloroform and then chloroform/methanol = 5/1 v/v) followed by purification on a Sephadex LH20 column (eluant: methanol) to afford the product (81 mg, 76%). ^{1}H NMR ($CDCl_3$, 400 MHz): δ(ppm) 2.49 (3H, s, CH_3CO), 7.53−7.57 (1H, m, C_6H_3), 7.86−7.94 (2H, m, C_6H_3). ^{19}F NMR ($CDCl_3$, 376 MHz): δ(ppm) −105.69 to −105.65.

2-Methoxy-4-acetylthiobenzoic Acid. 2-Methoxy-4-thiobenzoic acid (25 mg) was dissolved in diethyl ether/dichloromethane (1/1 v/v, 1.0 mL), and DIEA (35 μL) was added to the solution. Acetic anhydride (23 μL) was added to the solution at 0 °C under Ar atmosphere, and the solution was stirred at room

temperature for 26 h. The solution was diluted with chloroform and washed with 1 N aq HCl and brine, and the organic layer was dried over anhydrous $MgSO_4$. The $MgSO_4$ was filtered off, and the filtrate was subjected to preparative thin-layer chromatography to obtain the product (26 mg, 84%). ^{1}H NMR ($CDCl_3$, 400 MHz): δ(ppm) 2.45 (3H, s, CH_3CO), 4.01 (3H, s, OCH_3), 7.10−7.12 (2H, m, C$_6H_3$), 8.09 (1H, d, C$_6H_3$).

NL TLC (chloroform/methanol = 5/1 v/v). R_f = 0.72. ^{1}H NMR ($CDCl_3$, 400 MHz): δ(ppm) 0.8−1.1 (48H, LeuC$^\delta$H$_3$), 1.4−2.0 (72H, LeuC$^\beta$H$_2$, LeuC$^\gamma$H, AibCH$_3$), 2.45 (3H, CH$_3$CO), 3.3−3.8 (4H, NHCH$_2$CH$_2$NH), 3.8−4.1 (7H, LeuC$^\alpha$H), 4.1−4.4 (8H, LeuC$^\alpha$H, ferrocene-H), 4.7−5.1 (2H, ferrocene-H), 6.9−9.0 (22H, amide-NH, C$_6$H$_4$). MS (FAB, matrix; nitrobenzyl alcohol): *m/z* 2036.2 (calcd for $C_{102}H_{167}FeN_{18}O_{19}S$ [(M + H)$^+$] *m/z* 2036.2).

FL TLC (chloroform/methanol = 5/1 v/v). R_f = 0.57. ^{1}H NMR ($CDCl_3$, 400 MHz): δ(ppm) 0.8−1.1 (48H, LeuC$^\delta H_3$), 1.4−2.0 (72H, LeuC$^\beta H_2$, LeuC$^\gamma H$, AibCH_3), 2.47 (3H, CH_3CO), 3.2−3.5 (4H, NHCH_2CH_2NH), 3.8−4.1 (7H, LeuC$^\alpha H$), 4.1−4.4 (8H, LeuC$^\alpha H$, ferrocene-*H*), 4.7−5.0 (2H, ferrocene-*H*), 6.9−8.5 (21H, amide-N*H*, C$_6H_3$). MS (FAB, matrix; nitrobenzyl alcohol): *m/z* 2054.0 (calcd for $C_{102}H_{166}FFeN_{18}O_{19}S$ [(M + H)$^+$] *m/z* 2054.2).

ML TLC (chloroform/methanol = 5/1 v/v). R_f = 0.65. ^{1}H NMR ($CDCl_3$, 400 MHz): δ(ppm) 0.8−1.1 (48H, LeuC$^\delta H_3$), 1.4−2.0 (72H, LeuC$^\beta H_2$, LeuC$^\gamma H$, AibCH_3), 2.49 (3H, CH_3CO), 3.2−3.5 (4H, NHCH_2CH_2NH), 3.8−4.1 (11H, LeuC$^\alpha H$, OCH_3), 4.1−4.4 (7H, ferrocene-*H*), 4.7−5.0 (2H, ferrocene-*H*), 7.1−8.5 (21H, amide-N*H*, C$_6H_3$). MS (FAB, matrix; nitrobenzyl alcohol): *m/z* 2066.2 (calcd for $C_{103}H_{169}FeN_{18}O_{20}S$ [(M + H)$^+$] *m/z* 2066.2).

Preparation of SAMs. A slide glass was cleaned by sulfuric acid, rinsed with water and methanol, and dried in vacuum. A gold substrate was prepared by vapor deposition of chromium (300 Å) and then gold (99.99%, 2000 Å) onto the slide glass by a vacuum deposition system (N-KS350, Osaka Vacuum, Osaka). The prepared gold substrate was immediately used for self-assembling. The peptide was dissolved in ethanol (ca. 0.1 mM), and a 2 M dimethylamine in methanol solution (20−30 mol equiv of the peptide) was added to the solution to remove the acetyl group. The gold substrate was then immersed in the solution for 24 h. After that, the substrate was rinsed with ethanol, ethanol/chloroform (1/1 v/v), and chloroform in this order and dried in a N_2 stream and in vacuum for 15 min. In addition to these as-formed SAMs, SAMs whose defects were filled in with dodecanethiol were also prepared in two ways: immersion of the peptide SAM-modified substrates in a 0.3 mM dodecanethiol ethanol solution for 20 min or treatment of them with dodecanethiol vapor at 80 °C for 20 min.[52,64] After the treatment, the substrates were rinsed with ethanol, ethanol/chloroform (1/1 v/v), and chloroform in this order and dried in a N_2 stream and in vacuum for 15 min. One exception was the preparation of the NL SAM with treatment of dodecanethiol in a gas phase, where ammonia−water (25%, 300 mol equiv of the peptide) was used to remove the acetyl group, and the dodecanethiol treatment was for 2 h. At least three different monolayer samples were prepared for the respective nine different SAMs (three different peptides with three different treatments). All of them were subjected to the following measurements, and the results were averaged.

Monolayer Characterizations. IRRAS spectra were recorded on a Fourier transform infrared spectrometer (Nicolet 6700 FT-IR, Thermo Fisher Scientific, MA) at room temperature with a reflection attachment (RMA-1DG/VRA, Harrick, NY). The incident angle was set at 84° from the surface normal. The number of interferogram accumulations was 200. The tilt angles of the helix axis from the surface normal was determined from the amide I/II absorbance ratio by using an equation in the literature.[11,12,17,65,66] Ellipsometry was carried out by an autoellipsometer (DHA-OLX/S, Mizojiri Optical, Tokyo) at room temperature to determine the thicknesses of the monolayers. A helium−neon laser with a wavelength of 632.8 nm was used as the incident light at an incident angle of 65°. The complex optical constant of the monolayer was assumed to be 1.50 + 0.00*i*. The thickness of the monolayer was calculated automatically by an equipped program. The thicknesses were measured on more than five different spots on the substrate, and the data were averaged.

Electrochemical Measurements. Electrochemical experiments were performed by a voltammetric analyzer (model 604, BAS, Tokyo) at room temperature on a three-electrode system with the monolayer-modified gold substrate as the working electrode, Ag/AgCl in a 3 M NaCl aqueous solution as the reference electrode, and a platinum wire as the auxiliary electrode. Milli-Q water was used to prepare the solutions. The solutions were flushed with N_2 for 15 min prior to the experiments. All the applied potentials on the working electrode reported here are with respect to the reference electrode. The area of the working electrode exposed to the electrolyte solution was 0.9−1.1 cm^2. The uncompensated resistance of the cell, estimated by EIS, was ca. 3−4 Ω. The blocking experiment by CV to assess the monolayer defects was carried out in a 1 mM $K_4[Fe(CN)_6]$ and 1 M KCl aqueous solution at a scan rate of 0.1 V/s. The electron transfer experiments were carried out in a 1 M $HClO_4$ aqueous solution. CV was performed at various scan rates of 0.1−0.5 V/s. The capacitances of the monolayers were determined by dividing the current at 0.1 V, where the capacitive current is dominant, by the scan rate in the cyclic voltammograms of 0.1 V/s. In CA, the time constant in the current follower of the potentiostat was set at 10^{-4} s. The potential was stepped from formal oxidation potential − overpotential (V) to formal oxidation potential + overpotential (V) at time zero. EIS was performed with a DC voltage of 10 mV at frequencies from 10^5 to 1 Hz. The Bode plots obtained at the formal oxidation potential were fitted by an equivalent circuit shown in Figure 6 consisting of the solution resistance (R_s), monolayer constant phase element (CPE, $Z_{CPE} = (1/(Q(i\omega)^n))$), and electron-transfer resistance (R_{et}) and capacitance (C_{et}).[67−69] In this study, a CPE was used instead of a simple capacitance to get better agreement between the experimental and simulated curves by accounting for the inhomogeneity of the electrode surface.[70,71] The standard electron transfer rate constant (k_{et}^0) was calculated by $k_{et}^0 = 1/(2R_{et}C_{et})$.

Calculations of Molecular Length, Monolayer Thickness, and Monolayer Surface Density. The molecular length of the 16mer helical peptide was calculated to be 37.5 Å, while the distance between the ferrocene unit and gold along the molecule was estimated to be 31.5 Å in our previous work.[48] Thus, the theoretical thicknesses of the monolayers were calculated by 37.5 × cos(IRRAS tilt angle) (Å), and the direct distance between the ferrocene unit and gold along the surface normal was calculated by 31.5 × cos(IRRAS tilt angle) (Å). On the other hand, the theoretical peptide surface densities were estimated from the tilt angles and the limiting surface density which assumes hexagonal packing of helices with a 0° tilt angle. The limiting surface density was calculated to be 10.0×10^{-11}

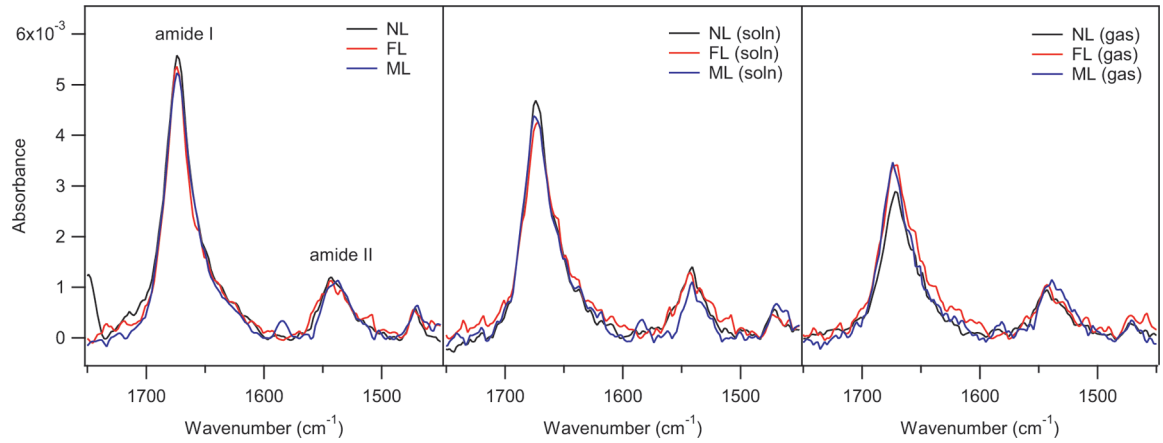

Figure 2. IRRAS spectra of the peptide SAMs.

TABLE 1: Summary of the Monolayer Characterizations

SAM	tilt angle (deg)	theoretical thickness from IRRAS (Å)	experimental thickness from ellipsometry (Å)	direct distance between ferrocene and gold from IRRAS (Å)
NL	30.9 ± 1.3	32.2 ± 0.5	22.1 ± 0.5	27.0 ± 0.4
NL (soln)	37.2 ± 0.7	29.9 ± 0.3	22.8 ± 0.7	25.1 ± 0.3
NL (gas)	37.9 ± 0.9	29.6 ± 0.4	21.5 ± 1.0	24.9 ± 0.3
FL	29.8 ± 1.3	32.5 ± 0.5	20.4 ± 0.7	27.3 ± 0.4
FL (soln)	35.4 ± 0.9	30.6 ± 0.3	18.7 ± 0.6	25.7 ± 0.3
FL (gas)	35.1 ± 2.0	30.7 ± 0.7	18.3 ± 0.3	25.8 ± 0.6
ML	34.4 ± 4.7	30.8 ± 1.8	17.2 ± 1.2	25.9 ± 1.5
ML (soln)	36.0 ± 2.6	30.4 ± 0.9	21.7 ± 0.5	25.5 ± 0.8
ML (gas)	39.1 ± 0.4	29.1 ± 0.2	22.9 ± 1.4	24.4 ± 0.2

mol/cm^2 as previously reported.[48] The limiting surface density × cos(IRRAS tilt angle) gave the theoretical peptide surface density.

Estimations of Oxidation Potentials of the Linkers and Peptide Chain. The oxidation potentials of the linkers and the amide group were estimated by ab initio quantum calculations. The model compounds in the calculations are 4-thiobenzoyl amide, 3-fluoro-4-thiobenzoyl amide, and 2-methoxy-4-thiobenzoyl amide for the linkers, and acetyl- and *N*-methylamide-protected glycine trimer for the amide group in a peptide chain, respectively. The initial geometries were generated by a CAChe WorkSystem software (ver. 6.1.1, Fujitsu, Tokyo) and optimized by the Molecular Mechanics program 2 (MM2), and the Austin Model 1 method (AM1) with the STO-3G basis set. The dihedral angles of the model peptide before the optimization were set to be $\omega = 180°$, $\phi = -67°$, and $\psi = -60°$ to generate an α-helix-like structure.[5] The obtained geometries were further optimized by the Hartree−Fock (HF) calculation with the 6-31 g(d) basis set and their single point energies were determined by the Becke's three parameter hybrid functional and Lee−Yang−Parr correlation (B3LYP) method with the 6-311+g(2d,p) basis set on a Gaussian03 program.[72] The series of calculations were performed for the natural state and cation state, and the energy difference between them after correction with the zero-point energies was determined as the calculated adiabatic ionization potential (IP_{calc}). According to the literature,[73] the oxidation potentials vs Ag/AgCl (E^0) were given by $E^0 = -4.88 + 0.82(IP_{calc} + 0.28) - 0.22$ V, where the last term is for correction of the reference electrodes from the standard hydrogen electrode to Ag/AgCl.

Results and Discussions

SAM Preparation and Characterization. The helical peptides (NL, FL, and ML; Figure 1) were synthesized by liquid-phase synthesis. The SAMs were prepared by immersion of a gold substrate into the respective peptide solutions after removing the acetyl group from the thiol group by a base treatment. To fill in monolayer defects, some of the prepared SAMs were treated with dodecanethiol from a solution or gas phase. These dodecanethiol-treated SAMs are labeled as "soln" and "gas", respectively.

Molecular orientation was examined by IRRAS spectroscopy. The spectra of the respective SAMs are shown in Figure 2. Amides I and II were observed at around 1670 cm^{-1} and 1540 cm^{-1}, respectively. These wave numbers are characteristic for helical conformation.[66] The tilt angles of the helices from the surface normal were determined on the basis of the ratio of the amide I and II absorbances.[11,12,17,65,66,74] The tilt angles are summarized in Table 1. The tilt angles are 30−34° for the as-formed SAMs, indicating that the helical peptides do not lie down on the surface but take an upright orientation. The treatments with dodecanethiol increased the tilt angles by 5−7°, suggesting that insertion of dodecanethiol molecules into the monolayer defects induces slight reorganization of the peptide molecules on the surface.[52] Moreover, the intensities of the amide absorptions decreased with the dodecanethiol treatment, showing that the peptides were partially replaced by the dodecanethiol molecules. The theoretical thicknesses of the SAMs were estimated from the molecular length (37.5 Å), and the tilt angles were determined by IRRAS (Table 1). The theoretical values roughly agree with the experimental monolayer thicknesses measured by ellipsometry (Table 1), showing that the peptides form a monolayer not a multilayer. Similarly, using the tilt angles, the direct distances between the ferrocene unit and gold along the surface normal (Table 1) and the theoretical peptide surface densities (Table 2) were also calculated.

TABLE 2: Summary of the Electrochemical Studies

SAM	experimental ferrocene surface density from CV ($\times 10^{-11}$ mol/cm^2)	theoretical peptide surface density from IRRAS ($\times 10^{-11}$ mol/cm^2)	k_{et}^0 from CA (s^{-1})	k_{et}^0 from EIS (s^{-1})	monolayer capacitance from CV (μF)
NL	10.4 ± 1.3	8.6 ± 0.1	–	44.2 ± 10.1	29.1 ± 7.8
NL (soln)	9.7 ± 0.3	8.0 ± 0.1	–	80.8 ± 16.3	17.5 ± 2.8
NL (gas)	5.5 ± 0.8	7.9 ± 0.1	14.9 ± 2.5	11.3 ± 1.9	10.5 ± 4.0
FL	11.3 ± 1.5	8.7 ± 0.1	–	26.6 ± 4.3	35.5 ± 6.8
FL (soln)	8.0 ± 0.7	8.2 ± 0.1	–	33.0 ± 10.8	16.1 ± 2.6
FL (gas)	6.8 ± 0.4	8.2 ± 0.2	20.4 ± 3.7	12.0 ± 2.0	8.5 ± 0.5
ML	4.1 ± 0.9	8.3 ± 0.3	–	8.6 ± 1.2	44.1 ± 6.3
ML (soln)	4.3 ± 0.3	8.1 ± 0.1	–	17.8 ± 1.1	20.5 ± 3.7
ML (gas)	3.6 ± 0.1	7.8 ± 0.5	17.8 ± 2.3	14.4 ± 1.8	9.7 ± 1.6

Electrochemical Measurements. To assess the monolayer defects, the SAMs were subjected to the blocking experiment which is cyclic voltammetry in an aqueous solution containing ferrocyanide redox ions. The results of a control bare gold substrate and the SAM-modified substrates are shown in Figure 3. The bare substrate shows clear redox peaks of the ferricyanide/ferrocyanide couple. The as-formed SAMs show noticeable redox peaks especially in the FL and ML SAMs, showing that there are bare regions exposed to the solution (pinholes) at which the redox ions can diffuse to the gold surface. On the other hand, in the "soln" SAMs, a peak current is hardly observed, and the voltammograms consist of a capacitive current (constant width between the anodic and cathodic currents) and tunneling current between the redox ions and gold through the monolayer (exponential rise of the current with the potential increase).[75] This shows that the majority of the pinholes were filled with dodecanethiol. Furthermore, in the "gas" SAMs, the capacitive current caused by water molecules and ion species inside the monolayer is remarkably reduced, showing that these monolayers are well-packed and nearly free from defects. It was demonstrated that the dodecanethiol treatment is effective to fill in the monolayer defects.

To study the electron transfer between the ferrocene unit and gold, cyclic voltammetry was performed in a $HClO_4$ solution. Figure 4 shows the cyclic voltammograms of the respective SAMs. In all the SAMs, reversible redox peaks of ferrocene oxidation are clearly observed, showing that the electron transfer occurs between the ferrocene unit and gold. The formal potentials for ferrocene oxidation are ca. 0.45 V in all the SAMs, and the peak separations are 20−30 mV. The anodic peak currents were found to be proportional to the scan rates (data not shown), confirming that the observed peaks arise from interfacial electron transfer between a surface-bound redox unit and the gold surface. The surface densities of the ferrocene unit were calculated by integration of the anodic peaks (Table 2). The ferrocene surface densities are slightly larger than the

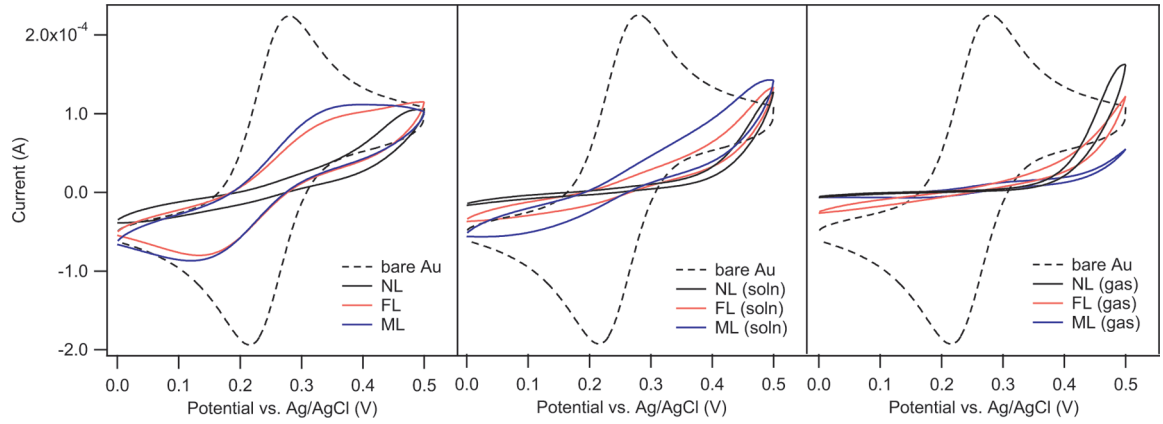

Figure 3. Cyclic voltammograms of a bare gold substrate and the SAM-modified substrates in a 1 mM $K_4[Fe(CN)_6]$ and 1 M KCl aqueous solution at a scan rate of 0.1 V/s.

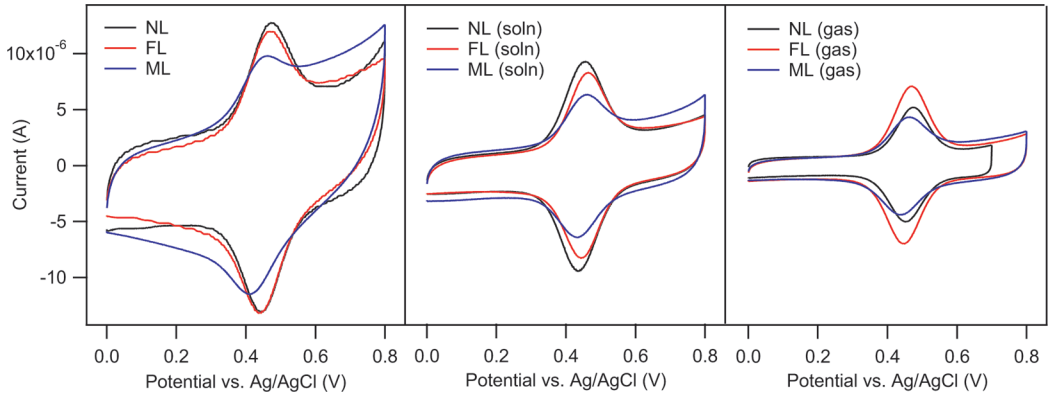

Figure 4. Cyclic voltammograms of the SAMs in a 1 M $HClO_4$ aqueous solution at a scan rate of 0.1 V/s.

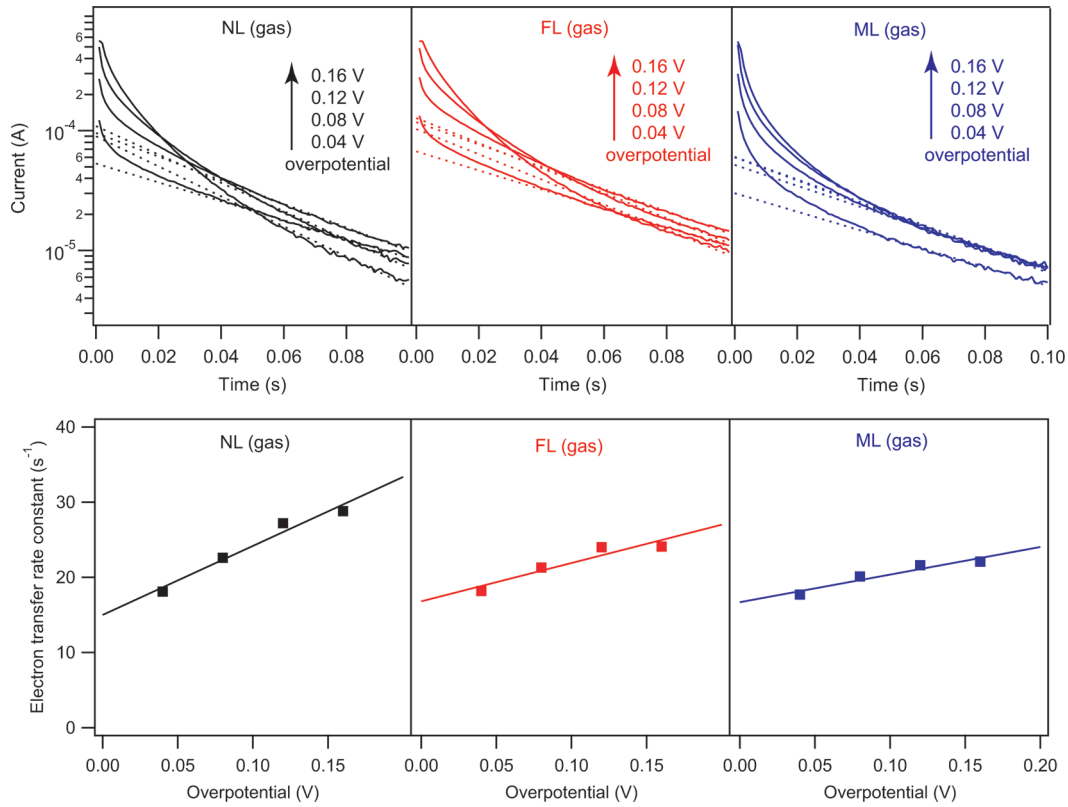

Figure 5. CA results: the current−time curves of the SAMs at various positive overpotentials applied at time zero in a semilog plot (upper panels), and the plots of the electron transfer rate constants over the overpotentials to determine the standard electron transfer rate constants (k_{et}^0) (lower panels).

theoretical peptide surface densities estimated from the helix tilt angles (Table 2) for the NL and FL as-formed SAMs, which can be explained by the surface roughness of a little larger than unity. On the other hand, the experimental ferrocene density in the ML SAM is about half of the theoretical peptide density, meaning that the peptide amount covalently bonded to gold is less than those of NL and FL. The electron-donating methoxy substituent on the linker may suppress the Au−S formation because of the unfavorable electrostatic effect on the polarization of the $Au^{\delta+}-S^{\delta-}$ bond,[76−78] which is in line with our previous result that a helical peptide with a linker at the negatively charged C-terminus formed a monolayer of less surface density than the case of a peptide with a linker at the N-terminus.[12] The dodecanethiol treatment remarkably reduced the capacitive current in the voltammograms, indicating the defects being filled in with dodecanethiol. At the same time, some part of the NL and FL SAMs should be replaced by dodeanethiol, because the ferrocene densities decreased with the treatment. In the case of the ML SAM, the filling in with dodecanthiol should mainly occur to the free space in the SAM rather than the replacement. Accidentally, the ferrocene densities of the three kinds of the peptide SAMs became comparable after the treatment with dodecanethiol in a gas phase.

With using the capacitive currents in the voltammograms as indicative of the momolayer packing (Table 2), the degree of the packing became tight in the order of as-formed SAMs < "soln" SAMs < "gas" SAMs, indicating that the monolayer defects were diminished by the dodecanethiol treatments. This trend is agreeable with the results of the blocking experiments. Most importantly, the capacitances of the "gas" SAMs were very close to each other among these three SAMs. It is therefore concluded that the dodecanethiol treatment in a gas phase successfully uniformed the ferrocene surface densities and monolayer capacitances among the three different SAMs.

CA was performed to determine the standard electron transfer rate constant (k_{et}^0). Time courses of the currents at various positive overpotentials in the "gas" SAMs are presented in the upper panels of Figure 5 in the form of a semilog plot. Each current−time curve has a linear part (0.04−0.10 s), the slope of which is the electron transfer rate constant (k_{et}).[79−81] The obtained k_{et} values were plotted versus the overpotentials (Figure 5 lower panels), and k_{et}^0 was determined by extrapolation to the zero overpotential (Table 2). On the other hand, similar CA measurements were unsuccessful for the as-formed SAMs and the "soln" SAMs because of large background currents which made it hard to find a linear region in the semilog plots. To supplement the CA results, EIS was carried out to determine k_{et}^0. The results obtained at the formal potential (0.45 V) are shown in Figure 6 as the Bode plots (absolute impedance and phase vs frequency). The Bode plots were analyzed by an equivalent circuit shown in the top panel of Figure 6 to determine the electron-transfer resistance (R_{et}) and capacitance (C_{et}), and the k_{et}^0 values were determined by $k_{et}^0 = 1/(2R_{et}C_{et})$. The results are summarized in Table 2. The k_{et}^0 values determined by EIS agree well with the values determined by CA, confirming the reliability of these measurements. Since the EIS measurements were successful on all the SAMs, the following discussion on the electron transfer is made on the basis of the EIS results.

The k_{et}^0 values determined by EIS are plotted against the direct distance between the ferrocene unit and gold along the surface normal (Figure 7a), the monolayer capacitances determined by CV (Figure 7b), and the ferrocene surface densities similarly determined by CV (Figure 7c). The direct distances are within a narrow distribution of ca. 2 Å among the three SAMs with the same treatment. However, the monolayer capacitances or ferrocene surface densities are quite different among the three peptides in the as-formed SAMs (circles, Figure

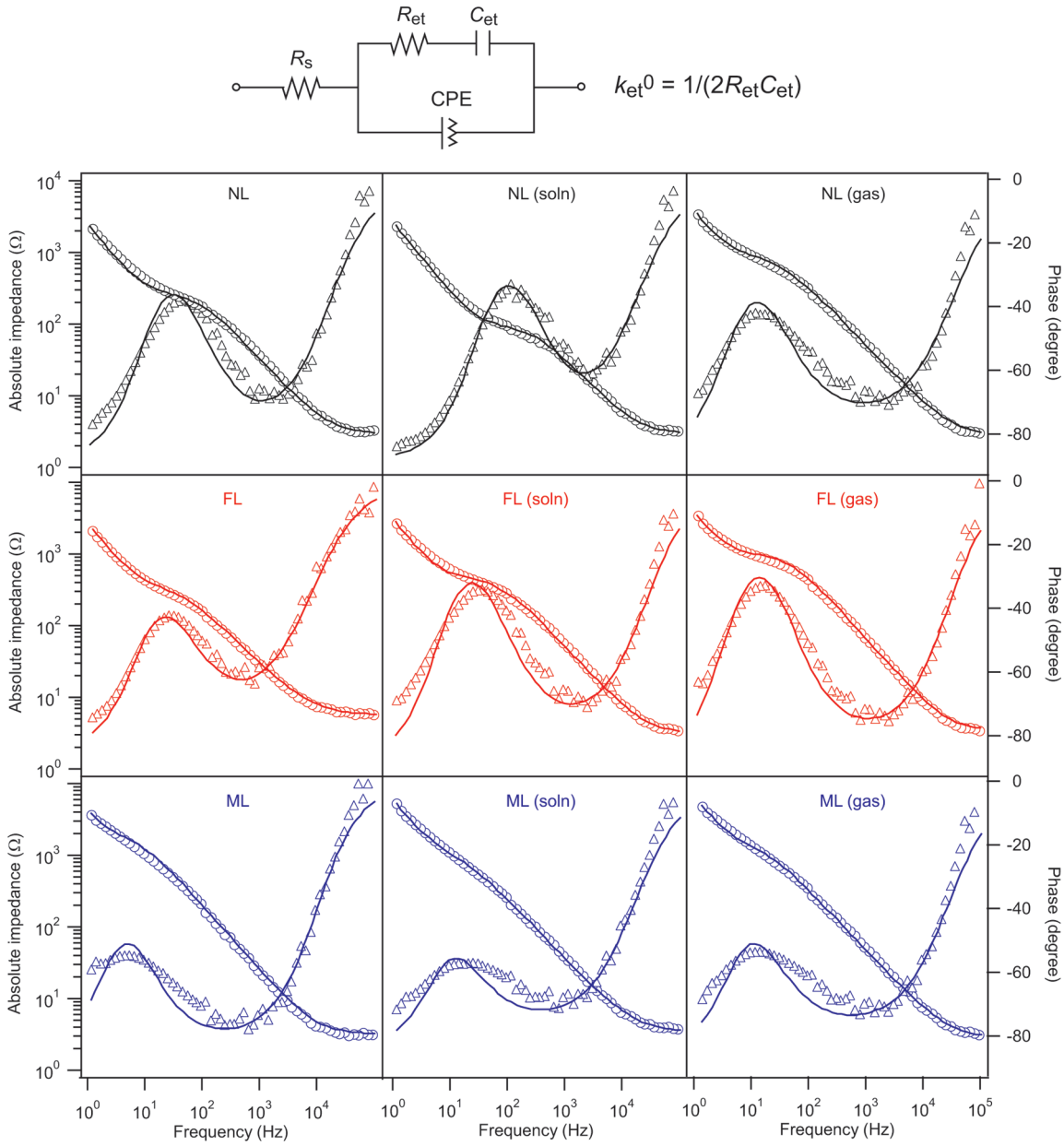

Figure 6. EIS results: an equivalent circuit used to analyze the EIS data (top), and the Bode plots of the SAMs at the ferrocene oxidation potential (0.45 V). The open circles and triangles show the experimental absolute impedance and phase, and the solid lines are the fitting curves.

7b, c) and the "soln" SAMs (triangles, Figure 7b, c). In contrast, these monolayer parameters are comparable in the "gas" SAMs among the three peptides (squares, Figure 7b, c). For extraction of the electronic effect of the linker on electron transfer, the k_{et}^0 values should be compared among the SAMs of similar physical qualities. The k_{et}^0 values of the "gas" SAMs are therefore used for the evaluation of the electronic effect of the linker, indicating there is no noticeable difference in these three SAMs, which are 11.3 ± 1.9 s^{-1} for the NL, 12.0 ± 2.0 s^{-1} for the FL, and 14.4 ± 1.8 s^{-1} for the ML SAMs, respectively. Notably, the deviations in the monolayer parameters (lateral error bars) and the deviations in the k_{et}^0 values (vertical error bars) are significantly small, showing high reproducibility of these values due to the reduction of background currents by the dodecanthiol treatment in a gas phase.

Theoretical Calculation on Electron Tunneling. It is concluded that the k_{et}^0 values are statistically the same among the three SAMs. For a quantitative discussion based on electron tunneling and hopping mechanisms, the oxidation potentials of the linkers and the amide group in a peptide chain were theoretically estimated by ab initio quantum calculations. Since the HOMOs of the linkers and the amide group are closer to the gold Fermi level than their LUMOs, we presume hole transfer in both tunneling and hopping mechanisms. The model compounds are 4-thiobenzoyl amide, 3-fluoro-4-thiobenzoyol amide, and 2-methoxy-4-thiobenzoyl amide for the linkers of NL, FL, and ML, and acetyl- and *N*-methylamide-protected glycine trimer for the amide group in a peptide chain, respectively. The first amide group at the N-terminus was included into the linker in these calculations because of its conjugation with the phenyl ring. The geometry of each compound was optimized in the AM1/STO-3G and then HF/6-31 g(d) levels in natural and cation forms, and their single point energies were determined by the B3LYP/6-311+g(2d,p) calculation. The energy difference between the natural and cation forms after correction with the zero-point energies is the calculated adiabatic ionization potential. The oxidation potentials vs Ag/AgCl were estimated from the calculated ionization

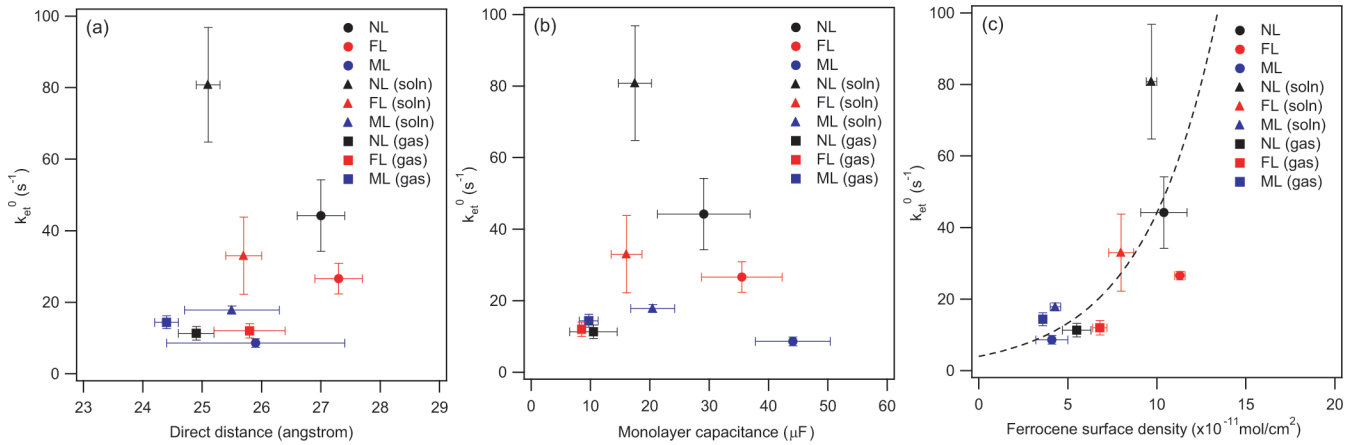

Figure 7. Relationships of k_{et}^0 with the direct distances between the ferrocene unit and gold (a), the monolayer capacitances determined by CV (b), and the ferrocene surface densities (c).

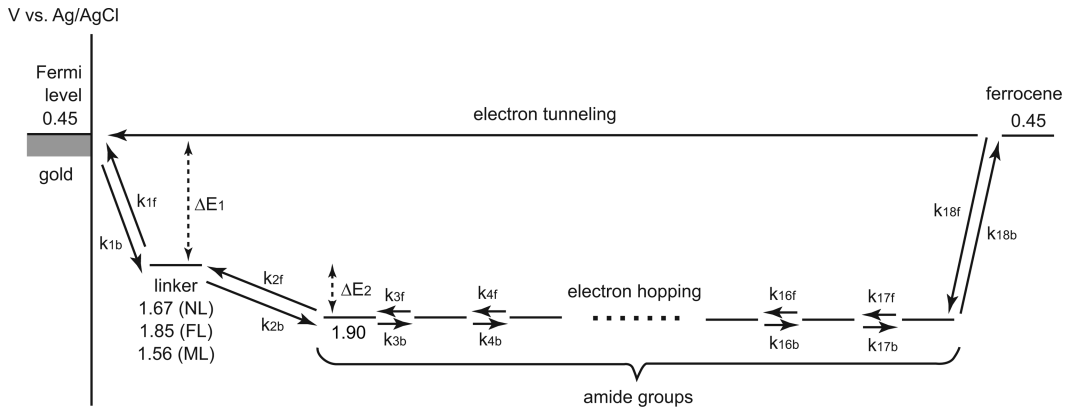

Figure 8. Energy diagram of the electron transfer from the ferrocene unit to gold through the helical peptide monolayer by electron tunneling and hopping mechanisms.

potentials using an equation in the literature[73] to be 1.67 V for 4-thiobenzoyl amide, 1.85 V for 3-fluoro-4-thiobenzoyl amide, 1.56 V for 2-methoxy-4-thiobenzoyl amide, and 1.90 V for the amide group in a peptide chain, respectively (Figure 8).

First, electron tunneling is considered using the Simmons model.[82] In the model, the electron tunneling probability (P_{et}) under a low bias is expressed by eq 1,[83−85]

$$P_{et} \propto \frac{\sqrt{2m\Delta E_1 e^2 \alpha}}{h^2 d} \exp\left[-\frac{4\pi\sqrt{2m}}{h}\alpha\sqrt{\Delta E_1 d}\right] \qquad (1)$$

where m is the electron mass, ΔE_1 the barrier height for electron tunneling, e the electron charge, α an adjustable parameter set to be 0.5 here, h the Planck's constant, and d the tunneling distance set to be 7 Å as an approximate length of the linker region, respectively. Since the electron tunneling path is the same among the three peptides besides the linker part, the electron transfer rate is considered proportional to the tunneling probability across the linker region. The barrier heights for hole tunneling were assumed to be 1.22 eV for NL, 1.40 eV for FL, and 1.11 eV for ML with the gold Fermi level of 0.45 V. The oxidation potentials were conveniently used here instead of the HOMO energies, because the gold Fermi level is changed by the applied potential and thus the relationships between the gold work function and the linker's HOMO levels cannot be used here. Using these barrier heights, the ratio of the tunneling probabilities was calculated to be 1.00:0.18:3.00 for NL:FL:ML, which does not fit the experimental result. However, the Simmons model is quite simple, and it is known that the model often fails to quantitatively explain the experimental results. For example, molecular conductances of 1,4-benzenedithiol with various substituents have been determined by the scanning-tunneling microscopy (STM) break-junction measurements.[86] The compounds were connected to two gold electrodes with Au−S linkages. The study revealed that the conductance of 2,3,5,6-tetrafluoro-1,4-benzendithiol is only about 20% less than that of 1,4-benzenedithiol despite its substantially lowered HOMO level. Another example is similar STM break-junction measurements on diamine derivatives with various oxidation potentials.[87] In the study, Au−NH_2 linkages were used to make metal−molecule−metal junctions. Comparison between 1,4-diaminobenzene, 1,4-diaminonaphthalene, and 9,10-diaminoanthracene shows that upon ca. 0.2 V increase in the oxidation potential, the molecular conductance is decreased only by half. These experimental results indicate that the Simmons model tends to overestimate the effect of frontier orbital energy on the tunneling probability. Therefore, although the calculations with the Simmons model have suggested that the electron transfer in the present SAMs is not governed by electron tunneling, electron tunneling cannot be fully excluded as the responsible mechanism.

Theoretical Calculation on a Hopping Mechanism. An electron hopping mechanism is considered. The hopping processes are shown in Figure 8. It is reasonable to consider that not only the amide groups but also the linker acts as a hopping site because its oxidation potential is located between the gold Fermi level and the amide oxidation potential.

According to the literature,[43] the standard rate constant of the overall electron transfer (k_{et}^0) by the hole hopping among the amide groups and the linker is expressed by eq 2 using the rate constants of the elementary electron transfer reactions shown in Figure 8.

$$k_{et}^0 = \frac{(k_{1f}/k_{1b})\Psi}{(1/k_{18f}) + (\Psi/k_{1b}) + ((1 + \Phi)/k_{19b})}, \quad \Psi = \prod_{i=2}^{17} \frac{k_{if}}{k_{ib}}, \quad \Phi = \sum_{j=2}^{16}\left(\prod_{i=j}^{16} \frac{k_{i+1f}}{k_{ib}}\right) \quad (2)$$

For simplicity here, it is assumed all the amide groups have the same oxidation potential, and thus $k_{if} = k_{ib} = k_{hop}$ (i = 3−17). Considering the energy differences between the respective hopping sites, $k_{1b} \gg k_{2f}$, $k_{2b} \gg k_{hop}$, and $k_{18f} \gg k_{hop}$. Under these conditions, eq 2 is simplified into eq 3.

$$k_{et}^0 \approx \frac{k_{1f}}{k_{1b}}\frac{k_{2f}}{k_{2b}}\frac{k_{hop}}{16} \quad (3)$$

Using formulas for metal−molecule and molecule−molecule electron transfer reactions,[38] k_{1f}/k_{1b} and k_{2f}/k_{2b} can be expressed by ΔE_1 and ΔE_2, and thus finally the rate constant is given by eq. 4,

$$k_{et}^0 \approx \exp\left[-\frac{\Delta E_1 + \Delta E_2}{k_B T}\right]\frac{k_{hop}}{16} \quad (4)$$

where k_B is the Boltzmann's constant and T is the temperature. ($\Delta E_1 + \Delta E_2$) is constant irrespective of the position of the oxidation potential of the linker as long as it is located between the gold Fermi level and the amide oxidation potential. Therefore, the experimental result is in line with the hopping mechanism.

The hole hopping phenomenon among amide groups in a peptide chain has been experimentally and theoretically studied by many groups. Two-photon ionization experiments of a peptide chain in a gas phase demonstrated that a photogenerated hole at an aromatic residue efficiently migrated to a distant site separated by a few amino acid residues,[88,89] and a so-called "ratcheting mechanism" was proposed[90,91] where a peptide backbone thermally fluctuates to have a specific geometry for the hole hopping due to the strong electronic coupling among neighboring amide groups and the diminished activation energy. For example, a three-electron bond between neighboring carbonyl oxygen atoms was recently proposed for the hole carrier.[92] There are other several reports showing that a facile hole transfer among amide groups is possible without accompanying any significant change in the peptide conformation. Theoretical calculations showed that neighboring amide groups have substantial electronic coupling in helical conformation[5] for the hole to transfer at a rate constant of ca. 10^{10} s^{-1}.[93] Even ultrafast hole transfer by electron correlation of a time constant of a few femtoseconds was also theoretically predicted.[94,95]

However, it should be noted that the rate constant simply calculated by eq 4 gives an unrealistic value ($<10^{-14}$ s^{-1}) even if a very fast electron hopping among the amide groups is assumed ($k_{hop} = 10^{10}$ s^{-1}), because of the large energy gap between the gold Fermi level and the amide oxidation potential ($\Delta E_1 + \Delta E_2 = 1.45$ V). This energy gap, however, should be overestimated because several factors which reduce the energy gap are neglected. For example, one of them is image dipole formation in gold to stabilize the cation of the amide group, which would reduce the energy gap as much as 1 eV especially near the gold surface.[36,37] Further, the cation form of an amide group has several ways to be stabilized by the surrounding peptidic environment.[91] These effects, which were not included in the calculation in this study, should lower the oxidation potential of the amide group. Furthermore, the hopping process among the amide groups should be promoted by the electric field generated by the peptide dipole, which is expressed as an energy slope along the amide groups, not a flat arrangement used in the calculation. However, it is difficult to include all these effects precisely into calculations at this moment. In this study, the focus is put on the effect of oxidation levels of the linkers on the electron transfer rate constants among the three SAMs, and thus the simplest model was used to extract the essence.

Other Features of the Electron Transfer. Our previous work showed that the exchange of linkers from lipoic acid with a methylene chain to thiobenzoic acid remarkably accelerated the electron transfer.[12] It is considered that the energy level of a methylene chain is far below the amide energy level, accordingly acting as a block rather than a hopping site to slow down the electron transfer. Another possibility is the difference in the surface densities of Au−S linkages in the two systems as described later. Now that it is confirmed that the linker does not affect the electron transfer, we can reexamine the experimental results presented in Figure 7 without concern for the difference in the linkers. There seems to be no correlation between the ferrocene−gold direct distance and the k_{et}^0 values (Figure 7a). Moreover, in the case of the as-formed and "soln" ML SAMs, the deviations in the k_{et}^0 values (vertical error bars) is negligible in spite of the quite large deviations in the direct distances (lateral error bars). It is thus suggested that the electron transfer does not depend on the molecular orientation; in other words, the electron transfer occurs intramolecularly. Correlation between the monolayer capacitances and the k_{et}^0 values is not recognized either (Figure 7b). These findings are in contrast to our previous work in which the molecular orientation and monolayer packing affected the electron transfer in Ala-Aib helical peptide SAMs through alteration of intermolecular electron transfer along a few peptides and molecular motion. This contrast can be accounted for by the peptide sequence difference. The Leu-Aib peptides used in this study carry bulky side chains which may act as a barrier against intermolecular electron transfer, and interdigitation among the side chains may suppress the molecular motion even in loosely packed monolayers with defects. On the other hand, an exponential or quadratic correlation is observed in the k_{et}^0 plot over the ferrocene surface density (Figure 7c). It appears that the electron transfer is decelerated by the decrease of the ferrocene surface density. There are three explanations in our mind. First, the surface density of the Au^+-S^- linkage increases as the peptides are replaced with dodecanethiol molecules of less cross-sectional area than helical peptides, and the enhanced electric field by the increased dipole of the Au^+-S^- linkage on the surface may somehow slow down the electron transfer. This explanation can be successfully applied to explanation of the above-mentioned previous result where the electron transfer was slower in a helical peptide immobilized on surface with a disulfide group (two Au−S linkages per one peptide) than in a helical peptide with a thiophenyl liker (one Au−S linkage per one peptide). However, this interpretation cannot explain the behavior of the

as-formed ML SAM which showed slow electron transfer without dodecanethiol treatment. Second, the electric field generated by the peptide dipole may be responsible. The electric field is proportional to the peptide surface density. The peptide dipoles direct to gold in a manner to accelerate the electron transfer in the present SAMs. The reduced electric field with decrease of the peptide surface density therefore slows down the electron transfer. Third, electron hopping among the ferrocene units may occur to deliver an electron to a substantially tilted helix in the disordered SAM, resulting in fast electron transfer to gold. If the electrons of the ferrocene units are first harvested to those sites via hopping among the ferrocene units to cause the fast electron transfer, the decrease of the ferrocene surface density would suppress the hopping to slow down the electron transfer. It is difficult to tell which interpretation is correct at this stage and there may be other causes as well. To clarify this k_{et}^0 dependence on the ferrocene surface density, further detailed investigation is needed.

Conclusions

We have studied the effect of linker, which connects a ferrocene-terminated helical peptide to a gold surface, on the long-range electron transfer across the helical peptide. Infrared spectroscopy and ellipsometry showed that the helical peptides form a monolayer with vertical orientation. To uniform the monolayer qualities among the three monolayers and to enable reproducible electron-transfer measurements, the monolayer defects were filled in with dodecanethiol. It was found that there is no significant effect by linkers on the electron transfer. Theoretical calculations with simple models showed that a hopping mechanism is more plausible than electron tunneling. However, some experimental results in the literature suggest that electron tunneling cannot be excluded. Furthermore, a few interesting features were revealed. In contrast to our previous study using alanine-based peptides, the effects on the electron transfer by the molecular orientation and monolayer packing were not recognized in this study with leucine-based peptides. Instead, the electron transfer was found to be decelerated by decrease of the ferrocene surface densities. We are now studying this surface-density dependence in depth. Also, we are working on temperature dependence, effects of the underlying metal, and distance dependence with much longer peptides along with theoretical calculations to identify the mechanism of long-range electron transfer through a helical peptide.

Acknowledgment. This work is partly supported by Grant-in-Aids for Young Scientists B (16750098), for Young Scientists A (20685009), for Exploratory Research (17655098), and for Scientific Research B (15350068), and by the Global COE program, International Center for Integrated Research and Advanced Education in Materials Science, from the Ministry of Education, Culture, Sports, Science, and Technology, Japan.

References and Notes

(1) Mayo, S. L.; Ellis, W. R.; Crutchley, R. J.; Gray, H. B. *Science* **1986**, *233*, 948–952.
(2) Beratan, D. N.; Onuchic, J. N.; Winkler, J. R.; Gray, H. B. *Science* **1992**, *258*, 1740–1741.
(3) Langen, R.; Chang, I. J.; Germanas, J. P.; Richards, J. H.; Winkler, J. R.; Gray, H. B. *Science* **1995**, *268*, 1733–1735.
(4) Isied, S. S. *Prog. Inorg. Chem.* **1984**, *32*, 443–517.
(5) Shin, Y. G. K.; Newton, M. D.; Isied, S. S. *J. Am. Chem. Soc.* **2003**, *125*, 3722–3732.
(6) Long, Y. T.; Abu-Rhayem, E.; Kraatz, H. B. *Chem.—Eur. J.* **2005**, *11*, 5186–5194.
(7) Hol, W. G. J. *Prog. Biophys. Mol. Biol.* **1985**, *45*, 149–195.
(8) Vassilian, A.; Wishart, J. F.; Vanhemelryck, B.; Schwarz, H.; Isied, S. S. *J. Am. Chem. Soc.* **1990**, *112*, 7278–7286.
(9) Ogawa, M. Y.; Wishart, J. F.; Young, Z. Y.; Miller, J. R.; Isied, S. S. *J. Phys. Chem.* **1993**, *97*, 11456–11463.
(10) Sisido, M.; Hoshino, S.; Kusano, H.; Kuragaki, M.; Makino, M.; Sasaki, H.; Smith, T. A.; Ghiggino, K. P. *J. Phys. Chem. B* **2001**, *105*, 10407–10415.
(11) Morita, T.; Kimura, S. *J. Am. Chem. Soc.* **2003**, *125*, 8732–8733.
(12) Watanabe, J.; Morita, T.; Kimura, S. *J. Phys. Chem. B* **2005**, *109*, 14416–14425.
(13) Galka, M. M.; Kraatz, H. B. *ChemPhysChem* **2002**, *3*, 356–359.
(14) Kraatz, H. B.; Bediako-Amoa, I.; Gyepi-Garbrah, S. H.; Sutherland, T. C. *J. Phys. Chem. B* **2004**, *108*, 20164–20172.
(15) Sek, S.; Tolak, A.; Misicka, A.; Palys, B.; Bilewicz, R. *J. Phys. Chem. B* **2005**, *109*, 18433–18438.
(16) Mandal, H. S.; Kraatz, H. B. *Chem. Phys.* **2006**, *326*, 246–251.
(17) Kai, M.; Takeda, K.; Morita, T.; Kimura, S. *J. Pept. Sci.* **2008**, *14*, 192–202.
(18) Xiao, X. Y.; Xu, B. Q.; Tao, N. J. *J. Am. Chem. Soc.* **2004**, *126*, 5370–5371.
(19) Sek, S.; Swiatek, K.; Misicka, A. *J. Phys. Chem. B* **2005**, *109*, 23121–23124.
(20) Sek, S.; Misicka, A.; Swiatek, K.; Maicka, E. *J. Phys. Chem. B* **2006**, *110*, 19671–19677.
(21) Antonello, S.; Formaggio, F.; Moretto, A.; Toniolo, C.; Maran, F. *J. Am. Chem. Soc.* **2003**, *125*, 2874–2875.
(22) Polo, F.; Antonello, S.; Formaggio, F.; Toniolo, C.; Maran, F. *J. Am. Chem. Soc.* **2005**, *127*, 492–493.
(23) Hsu, C. P. *J. Electroanal. Chem.* **1997**, *438*, 27–35.
(24) Xu, B. Q.; Tao, N. J. J. *Science* **2003**, *301*, 1221–1223.
(25) Liu, B.; Bard, A. J.; Mirkin, M. V.; Creager, S. E. *J. Am. Chem. Soc.* **2004**, *126*, 1485–1492.
(26) Morita, T.; Lindsay, S. *J. Am. Chem. Soc.* **2007**, *129*, 7262–7263.
(27) Fox, M. A.; Galoppini, E. *J. Am. Chem. Soc.* **1997**, *119*, 5277–5285.
(28) Galoppini, E.; Fox, M. A. *J. Am. Chem. Soc.* **1996**, *118*, 2299–2300.
(29) Yasutomi, S.; Morita, T.; Kimura, S. *J. Am. Chem. Soc.* **2005**, *127*, 14564–14565.
(30) Yasutomi, S.; Morita, T.; Imanishi, Y.; Kimura, S. *Science* **2004**, *304*, 1944–1947.
(31) Morita, T.; Kimura, S.; Kobayashi, S.; Imanishi, Y. *J. Am. Chem. Soc.* **2000**, *122*, 2850–2859.
(32) Malak, R. A.; Gao, Z. N.; Wishart, J. F.; Isied, S. S. *J. Am. Chem. Soc.* **2004**, *126*, 13888–13889.
(33) Dey, S. K.; Long, Y. T.; Chowdhury, S.; Sutherland, T. C.; Mandal, H. S.; Kraatz, H. B. *Langmuir* **2007**, *23*, 6475–6477.
(34) Petrov, E. G.; May, V. *J. Phys. Chem. A* **2001**, *105*, 10176–10186.
(35) Petrov, E. G.; Shevchenko, Y. V.; Teslenko, V. I.; May, V. *J. Chem. Phys.* **2001**, *115*, 7107–7122.
(36) Petrov, E. G.; Hanggi, P. *Phys. Rev. Lett.* **2001**, *86*, 2862–2865.
(37) Petrov, E. G.; May, V.; Hanggi, P. *Chem. Phys.* **2002**, *281*, 211–224.
(38) Adams, D. M.; Brus, L.; Chidsey, C. E. D.; Creager, S.; Creutz, C.; Kagan, C. R.; Kamat, P. V.; Lieberman, M.; Lindsay, S.; Marcus, R. A.; Metzger, R. M.; Michel-Beyerle, M. E.; Miller, J. R.; Newton, M. D.; Rolison, D. R.; Sankey, O.; Schanze, K. S.; Yardley, J.; Zhu, X. Y. *J. Phys. Chem. B* **2003**, *107*, 6668–6697.
(39) Segal, D.; Nitzan, A.; Davis, W. B.; Wasielewski, M. R.; Ratner, M. A. *J. Phys. Chem. B* **2000**, *104*, 3817–3829.
(40) Berlin, Y. A.; Burin, A. L.; Ratner, M. A. *J. Am. Chem. Soc.* **2001**, *123*, 260–268.
(41) Berlin, Y. A.; Burin, A. L.; Ratner, M. A. *Chem. Phys.* **2002**, *275*, 61–74.
(42) Berlin, Y. A.; Hutchison, G. R.; Rempala, P.; Ratner, M. A.; Michl, J. *J. Phys. Chem. A* **2003**, *107*, 3970–3980.
(43) Berlin, Y. A.; Ratner, M. A. *Radiat. Phys. Chem.* **2005**, *74*, 124–131.
(44) Davis, W. B.; Ratner, M. A.; Wasielewski, M. R. *J. Am. Chem. Soc.* **2001**, *123*, 7877–7886.
(45) Weiss, E. A.; Ahrens, M. J.; Sinks, L. E.; Gusev, A. V.; Ratner, M. A.; Wasielewski, M. R. *J. Am. Chem. Soc.* **2004**, *126*, 5577–5584.
(46) Weiss, E. A.; Tauber, M. J.; Kelley, R. F.; Ahrens, M. J.; Ratner, M. A.; Wasielewski, M. R. *J. Am. Chem. Soc.* **2005**, *127*, 11842–11850.
(47) Orlowski, G. A.; Chowdhury, S.; Kraatz, H. B. *Langmuir* **2007**, *23*, 12765–12770.
(48) Takeda, K.; Morita, T.; Kimura, S. *J. Phys. Chem. B* **2008**, *112*, 12840–12850.
(49) Sek, S.; Sepiol, A.; Tolak, A.; Misicka, A.; Bilewicz, R. *J. Phys. Chem. B* **2004**, *108*, 8102–8105.
(50) Kitagawa, K.; Morita, T.; Kimura, S. *J. Phys. Chem. B* **2005**, *109*, 13906–13911.

(51) Kitagawa, K.; Morita, T.; Kimura, S. *Langmuir* **2005**, *21*, 10624–10631.
(52) Morita, T.; Yanagisawa, K.; Kimura, S. *Polym. J.* **2008**, *40*, 700–709.
(53) Yanagisawa, K.; Morita, T.; Kimura, S. *J. Am. Chem. Soc.* **2004**, *126*, 12780–12781.
(54) Tada, Y.; Morita, T.; Umemura, J.; Iwamoto, M.; Kimura, S. *Polym. J.* **2005**, *37*, 599–607.
(55) Kitagawa, K.; Morita, T.; Kimura, S. *Angew. Chem., Int. Ed.* **2005**, *117*, 6488–6491.
(56) Wakabayashi, M.; Fujii, S.; Morita, T.; Kimura, S. *Chem. Lett.* **2008**, *37*, 702–703.
(57) Chidsey, C. E. D. *Science* **1991**, *251*, 919–922.
(58) Sikes, H. D.; Smalley, J. F.; Dudek, S. P.; Cook, A. R.; Newton, M. D.; Chidsey, C. E. D.; Feldberg, S. W. *Science* **2001**, *291*, 1519–1523.
(59) Smalley, J. F.; Finklea, H. O.; Chidsey, C. E. D.; Linford, M. R.; Creager, S. E.; Ferraris, J. P.; Chalfant, K.; Zawodzinsk, T.; Feldberg, S. W.; Newton, M. D. *J. Am. Chem. Soc.* **2003**, *125*, 2004–2013.
(60) Smalley, J. F.; Sachs, S. B.; Chidsey, C. E. D.; Dudek, S. P.; Sikes, H. D.; Creager, S. E.; Yu, C. J.; Feldberg, S. W.; Newton, M. D. *J. Am. Chem. Soc.* **2004**, *126*, 14620–14630.
(61) Creager, S.; Yu, C. J.; Bamdad, C.; O'Connor, S.; MacLean, T.; Lam, E.; Chong, Y.; Olsen, G. T.; Luo, J. Y.; Gozin, M.; Kayyem, J. F. *J. Am. Chem. Soc.* **1999**, *121*, 1059–1064.
(62) Kitagawa, K.; Morita, T.; Kawasaki, M.; Kimura, S. *J. Polym. Sci., Part A: Polym. Chem.* **2003**, *41*, 3493–3500.
(63) Kitagawa, K.; Morita, T.; Kimura, S. *J. Phys. Chem. B* **2004**, *108*, 15090–15095.
(64) Donhauser, Z. J.; Mantooth, B. A.; Kelly, K. F.; Bumm, L. A.; Monnell, J. D.; Stapleton, J. J.; Price, D. W.; Rawlett, A. M.; Allara, D. L.; Tour, J. M.; Weiss, P. S. *Science* **2001**, *292*, 2303–2307.
(65) Gremlich, H. U.; Fringeli, U. P.; Schwyzer, R. *Biochemistry* **1983**, *22*, 4257–4264.
(66) Kennedy, D. F.; Crisma, M.; Toniolo, C.; Chapman, D. *Biochemistry* **1991**, *30*, 6541–6548.
(67) Steinem, C.; Janshoff, A.; Ulrich, W. P.; Sieber, M.; Galla, H. J. *Biochim. Biophys. Acta* **1996**, *1279*, 169–180.
(68) Yamada, T.; Nango, M.; Ohtsuka, T. *J. Electroanal. Chem.* **2002**, *528*, 93–102.
(69) Creager, S. E.; Wooster, T. T. *Anal. Chem.* **1998**, *70*, 4257–4263.
(70) Wu, X. Z.; Zhang, W. Z.; Hou, Y. *J. Electroanal. Chem.* **1995**, *398*, 1–4.
(71) Protsailo, L. V.; Fawcett, W. R. *Electrochim. Acta* **2000**, *45*, 3497–3505.
(72) Frisch, M. J.; Trucks, G. W.; Schlegel, H. B.; Scuseria, G. E.; Robb, M. A.; Cheeseman, J. R.; A., M. J. J.; Vreven, T.; Kudin, K. N.; Burant, J. C.; Millam, J. M.; Iyengar, S. S.; Tomasi, J.; Barone, V.; Mennucci, B.; Cossi, M.; Scalmani, G.; Rega, N.; Petersson, G. A.; Nakatsuji, H.; Hada, M.; Ehara, M.; Toyota, K.; Fukuda, R.; Hasegawa, J.; Ishida, M.; Nakajima, T.; Honda, Y.; Kitao, O.; Nakai, H.; Klene, M.; Li, X.; Knox, J. E.; Hratchian, H. P.; Cross, J. B.; Adamo, C.; Jaramillo, J.; Gomperts, R.; Stratmann, R. E.; Yazyev, O.; Austin, A. J.; Cammi, R.; Pomelli, C.; Ochterski, J. W.; Ayala, P. Y.; Morokuma, K.; Voth, G. A.; Salvador, P.; Dannenberg, J. J.; Zakrzewski, V. G.; Dapprich, S.; Daniels, A. D.; Strain, M. C.; Farkas, O.; Malick, D. K.; Rabuck, A. D.; Raghavachari, K.; Foresman, J. B.; Ortiz, J. V.; Cui, Q.; Baboul, A. G.; Clifford, S.; Cioslowski, J.; Stefanov, B. B.; Liu, G.; Liashenko, A.; Piskorz, P.; Komaromi, I.; Martin, R. L.; Fox, D. J.; Keith, T.; Al-Laham, M. A.; Peng, C. Y.; Nanayakkara, A.; Challacombe, M.; Gill, P. M. W.; Johnson, B.; Chen, W.; Wong, M. W.; Gonzalez, C.; Pople, J. A. Gaussian03; Gaussian Inc., Wallingford, CT, 2004.
(73) Fu, Y.; Liu, L.; Yu, H. Z.; Wang, Y. M.; Guo, Q. X. *J. Am. Chem. Soc.* **2005**, *127*, 7227–7234.
(74) Tsuboi, M. *J. Polym. Sci.* **1962**, *59*, 139.
(75) Finklea, H. O. In *Electroanalytical Chemistry*; Bard, A. J., Rubinstein, I., Eds.; Marcel Dekker: New York, 1993; Vol. 19, pp 177−220.
(76) Sellers, H.; Ulman, A.; Shnidman, Y.; Eilers, J. E. *J. Am. Chem. Soc.* **1993**, *115*, 9389–9401.
(77) Biebuyck, H. A.; Whitesides, G. M. *Langmuir* **1993**, *9*, 1766–1770.
(78) Biebuyck, H. A.; Bian, C. D.; Whitesides, G. M. *Langmuir* **1994**, *10*, 1825–1831.
(79) Finklea, H. O.; Ravenscroft, M. S.; Snider, D. A. *Langmuir* **1993**, *9*, 223–227.
(80) Finklea, H. O.; Hanshew, D. D. *J. Am. Chem. Soc.* **1992**, *114*, 3173–3181.
(81) Sek, S.; Palys, B.; Bilewicz, R. *J. Phys. Chem. B* **2002**, *106*, 5907–5914.
(82) Simmons, J. G. *J. Appl. Phys.* **1963**, *34*, 1793–1803.
(83) Holmlin, R. E.; Haag, R.; Chabinyc, M. L.; Ismagilov, R. F.; Cohen, A. E.; Terfort, A.; Rampi, M. A.; Whitesides, G. M. *J. Am. Chem. Soc.* **2001**, *123*, 5075–5085.
(84) Wang, W. Y.; Lee, T.; Reed, M. A. *Phys. Rev. B* **2003**, *68*, 035416.
(85) Lee, T.; Wang, W. Y.; Klemic, J. F.; Zhang, J. J.; Su, J.; Reed, M. A. *J. Phys. Chem. B* **2004**, *108*, 8742–8750.
(86) Baheti, K.; Malen, J. A.; Doak, P.; Reddy, P.; Jang, S. Y.; Tilley, T. D.; Majumdar, A.; Segalman, R. A. *Nano Lett.* **2008**, *8*, 715–719.
(87) Quinn, J. R.; Foss, F. W.; Venkataraman, L.; Breslow, R. *J. Am. Chem. Soc.* **2007**, *129*, 12376–12377.
(88) Weinkauf, R.; Schanen, P.; Yang, D.; Sonkara, S.; Schlag, E. W. *J. Phys. Chem.* **1995**, *99*, 11255–11265.
(89) Weinkauf, R.; Schanen, P.; Metsala, A.; Schlag, E. W.; Burgle, M.; Kessler, H. *J. Phys. Chem.* **1996**, *100*, 18567–18585.
(90) Baranov, L. Y.; Schlag, E. W. *Z. Naturforsch.* **1999**, *54a*, 387–396.
(91) Schlag, E. W.; Sheu, S. Y.; Yang, D. Y.; Selzle, H. L.; Lin, S. H. *Angew. Chem., Int. Ed.* **2007**, *46*, 3196–3210.
(92) Chen, X. H.; Zhang, L.; Wang, Z. P.; Li, J. L.; Wang, W.; Bu, Y. X. *J. Phys. Chem. B* **2008**, *112*, 14302–14311.
(93) Santhanamoorthi, N.; Kolandaivel, P.; Senthilkumar, K. *J. Phys. Chem. A* **2006**, *110*, 11551–11556.
(94) Hennig, H.; Breidbach, J.; Cederbaum, L. S. *J. Phys. Chem. A* **2005**, *109*, 409–414.
(95) Kuleff, A. I.; Breidbach, J.; Cederbaum, L. S. *J. Chem. Phys.* **2005**, *123*, 044111.

JP810200X